Interpretation of NH 3 -TPD Profiles from Cu-CHA Using First-Principles Calculations

Topics in Catalysis (2019) 62:93–99
https://doi.org/10.1007/s11244-018-1095-y

ORIGINAL ARTICLE

Interpretation of NH_3-TPD Profiles from Cu-CHA Using First-Principles Calculations

Lin Chen[1] · Ton V. W. Janssens[2] · Magnus Skoglundh[1] · Henrik Grönbeck[1]

Published online: 26 November 2018

Abstract
Temperature-programmed desorption (TPD) with ammonia is widely used for zeolite characterization revealing information on acidity and adsorption sites. The interpretation of TPD measurements is, however, often challenging. One example is the NH_3-TPD profile from Cu-chabazite (Cu-CHA) which generally is deconvoluted in three peaks with contributions from NH_3 on Lewis acid sites, copper sites and Brønsted acid sites. Here, we use density functional theory calculations combined with kinetic simulations to analyze this case. We find a large number of possible species, giving rise to overlapping features in the NH_3-TPD. The experimental low-temperature peak (below 200 °C) is assigned to NH_3 desorption from Lewis acid sites together with NH_3 desorption from a $[Cu(II)(OH)(NH_3)_3]^+$ complex. The intermediate-temperature peak (250−350 °C) is attributed to decomposition of a linear $[Cu(I)(NH_3)_2]^+$ complex and a residual from $[Cu(II)(OH)(NH_3)_3]^+$. The high-temperature peak is predicted to have contributions from Brønsted acid sites (NH_4^+), $[Cu(I)NH_3]^+$ and $[Cu(II)(NH_3)_4]^{2+}$. The present work shows that NH_3-TPD from Cu-CHA can be reconciled with copper complexes as NH_3 storage sites.

Keywords NH_3-TPD · Zeolites · Cu-CHA · Acidity

1 Introduction

Temperature-programmed desorption (TPD) is widely used for characterization of heterogeneous catalysts. The method is straightforward and based on the measurement of the desorption profile of a pre-adsorbed probe molecule during controlled heating. For zeolites and oxide surfaces, NH_3-TPD is generally used to measure the amount of acid sites together with the acid strength [1, 2]. Despite its simplicity, the interpretation of TPD profiles is often hampered by limited knowledge on the active sites, sample heterogeneity and coverage dependent adsorbate–adsorbate interactions. Due to these complications, TPD measurements are commonly used merely as a catalyst signature of acidity rather than a means to obtain site-specific information. One example is NH_3-TPD profiles from zeolites functionalized with copper ions.

Zeolites exchanged with copper ions are efficient catalysts for selective catalytic reduction of NO_x with ammonia (NH_3-SCR), which is the basis of the current technology for the abatement of NO_x emission from diesel engines [3, 4]. In particular, copper-exchanged zeolites and zeotypes with the small-pore chabazite framework structure (Cu-CHA) is the state-of-the-art catalyst for NH_3-SCR which combines a good performance in the temperature range 200−550 °C with a high hydrothermal stability [5–7]. The NH_3-TPD profile of Cu-CHA is characterized by three desorption peaks [8–17]; a low-temperature peak below 200 °C, an intermediate-temperature peak at 250−350 °C and a high-temperature peak at 400−500 °C.

The low-temperature peak is generally assigned to NH_3 adsorbed to Lewis acid sites [8–13, 17] whereas the peak at 400−500 °C has been attributed to NH_3 adsorbed on Brønsted acid sites. NH_3 adsorbed at Cu-sites has been suggested to give rise to the intermediate-temperature peak at 250−350 °C [8–12]. An attempt to assign the peaks to specific Cu sites was made in Ref. [8] where the intermediate and high temperature peaks were attributed to Cu

✉ Lin Chen
clin@chalmers.se

✉ Henrik Grönbeck
ghj@chalmers.se

[1] Department of Physics and Competence Centre for Catalysis, Chalmers University of Technology, 412 96 Göteborg, Sweden

[2] Umicore Denmark ApS, Nøjsomhedsvej 20, 2800 Kongens Lyngby, Denmark

coordinated to the zeolite framework in 6- and 8-membered rings, respectively.

The understanding of the active sites in Cu-CHA during operating conditions has advanced during the recent years. Experimental as well as computational studies have shown that Cu^+ is preferably solvated by two NH_3 ligands forming a linear $[Cu(I)(NH_3)_2]^+$ complex under low-temperature NH_3-SCR conditions [18–24]. The $[Cu(I)(NH_3)_2]^+$ complex is mobile with low barriers for inter-cage diffusion and suggested to be important also for the solid-state ion-exchange reaction [25]. In addition to Cu^+ species, Cu-CHA also contain solvated Cu^{2+} species in the form of $[Cu(II)(NH_3)_4]^{2+}$ or $[Cu(II)(OH)(NH_3)_3]^+$ [15, 18, 20].

The evidence of NH_3-solvated complexes under NH_3-SCR conditions should have consequences for the interpretation of NH_3-TPD profile from Cu-CHA. In particular, the desorbed NH_3 should partly originate from NH_3-solvated Cu-complexes. In this study, density functional theory calculations in combination with kinetic simulations are used to elucidate the NH_3-TPD profile from Cu-CHA. We find that the experimental NH_3-TPD curves can be reconciled with NH_3 desorbing from Lewis acid sites, solvated copper species and Brønsted acid sites. By simulating the NH_3-TPD curves based on the stability of different species as calculated by DFT, we obtain insights on the observed features of NH_3-TPD from Cu-CHA. Moreover, the identification of the decomposition temperature of $[Cu(I)(NH_3)_2]^+$ complexes provides information that elucidates the temperature dependent activity of the Cu-CHA catalyst, including the often observed decrease in NO conversion with increasing temperature.

2 Computational Methods

2.1 Density Functional Theory Calculations

Spin-polarised density functional theory calculations are performed with the Vienna Ab-Initio Simulation Package (VASP) [26–29].[1] The Kohn–Sham orbitals are expanded with plane waves using an energy cut-off of 480 eV and the interaction between the valence electrons and the cores is described with the plane augmented wave (PAW) method [30, 31]. The number of valence electrons used in the calculations are 11 for Cu, 4 for Si, 3 for Al, 6 for O, 5 for N and 1 for H. The exchange-correlation functional is approximated with the PBE+cx van der Waals functional [32]. PBE+cx makes use of the vdW-DF [33] description, which provides an accurate description of binding energies of, for example, molecular dimers [32]. Structures are optimized with the conjugate gradient method and geometries are considered to be converged when the electronic energy difference between subsequent steps is smaller than 1×10^{-5} eV and the largest force is smaller than 3×10^{-2} eV/Å. The k-point sampling is restricted to the Γ-point. The calculated energies are zero-point corrected and the harmonic vibrational frequencies are computed using a finite-difference approach.

The chabazite structure is modeled using a rhombohedral unit cell which includes 12 Si atoms in tetrahedral (T) positions. The optimized cell parameters are a, b, c = 9.42 Å and $\alpha, \beta, \gamma = 94°$. The lattice parameters are kept fixed during the geometry relaxations.[2] The Si/Al ratio is 11 and 5 when considering cationic and double cationic species, respectively. Both Si/Al ratios are within the common experimental range between 20 and 5 [20, 34–36]. To study the influence of complex and adsorbate concentration, calculations were performed also in a $(2 \times 2 \times 2)$ super-cell increasing the Si/Al ratio by a factor of 8.

2.2 Evaluation of NH_3-TPD

The NH_3 desorption profiles have been analyzed following Refs. [37, 38] taking readsorption into account. Consequently, the simulated process is:

$$NH_3^* \underset{k_a}{\overset{k_d}{\rightleftharpoons}} NH_3(g) + * \tag{1}$$

where $*$ denotes an adsorption site and NH_3(g) is ammonia in the gas phase. k_d and k_a are the desorption and adsorption rate constants, respectively. In the mean-field assumption, the time derivative of the NH_3 coverage (θ) is given by:

$$\frac{d\theta}{dt} = k_a \frac{P_g}{P^0}(1-\theta) - k_d\theta \tag{2}$$

where P_g is the pressure of ammonia and P^0 is the pressure at standard conditions. Using the ideal gas law, P_g can be written as RTC_g where R is the gas constant, T is the temperature and C_g is the ammonia concentration. The concentration can be calculated assuming equilibrium between the gaseous and adsorbed ammonia:

$$C_g = \frac{\theta}{1-\theta}\frac{P^0}{RT}K \tag{3}$$

where K is the equilibrium constant given by the enthalpy and entropy changes (ΔH and ΔS) upon desorption:

[1] We used VASP version 5.4.1.

[2] We also performed tests with the $(1 \times 1 \times 1)$ unit cell relaxing the cell parameters. The volume of the relaxed cell is decreased by 1–4% depending on the considered complex. The adsorption energies are ~ 0.1 eV lower than for the case with a fixed cell. However, as the Cu loading in our calculations is much higher than in the experiments, the effect of relaxation is most likely overestimated.

$$K = \frac{k_d}{k_a} = \exp\left(-\frac{\Delta H}{RT}\right)\exp\left(\frac{\Delta S}{R}\right) \quad (4)$$

The mass balance in the flowing gas is:

$$FC_g = -A_0 W\frac{d\theta}{dt} = -\beta A_0 W\frac{d\theta}{dT} \quad (5)$$

where F is the flow rate of the carrier gas, A_0 is the concentration of the adsorption sites, W is the zeolite weight and β is the heating rate ($\Delta T = \beta\delta t$). The concentration can in this way be written:

$$C_g = -\frac{\beta A_0 W}{F}\frac{d\theta}{dT} = \frac{\theta}{1-\theta}\frac{P^0}{RT}\exp\left(-\frac{\Delta H}{RT}\right)\exp\left(\frac{\Delta S}{R}\right) \quad (6)$$

The concentration depends on temperature and site-coverage. The site-coverage is obtained iteratively through:

$$\theta_{i+1} = \theta_i + \left(\frac{d\theta}{dT}\right)_i \Delta T \quad (7)$$

This relation connects C_g and T, which gives the TPD profile.

The calculated NH_3-TPD profiles are compared to experimental data for a Cu-CHA catalyst with Si/Al = 15 and a Cu loading of 2.9 wt% Cu. The NH_3-TPD was measured with a microreactor system, using a 50 mg sample of the catalyst in a quartz U-tube (4 mm inner diameter). The flow rate was 190 Nml/min during the entire procedure. The catalyst was initially reduced in a mixture of 800 ppm NO and 900 ppm NH_3 at 200 °C; under these conditions the $[Cu(I)(NH_3)_2]^+$ complex is formed [39]. NO was thereafter removed from the gas phase, and the catalyst was saturated in 900 ppm NH_3 at 200 °C, followed by 2 h purge in N_2 at the same temperature. To measure the NH_3-TPD, the sample was cooled down to 150 °C, and thereafter heated to 550 °C at a rate of 3 °C/min, while the concentration of NH_3 in the reactor exit gas was recorded using a FTIR spectrometer (Gasmet CX4000) connected to the reactor outlet.

3 Results and Discussion

The desorption peaks in the TPD-profile are sensitive to the change in free energy ($\Delta G = \Delta H - T\Delta S$). The change in entropy (ΔS) has been measured to be close to constant (*ca* 150 J/K/mol) over a wide range of zeolites and experimental conditions [38], therefore we use this value. The change in enthalpy (ΔH) is here calculated using DFT. To verify the ability of the current approach to describe the interactions between Cu ions and NH_3, we calculated the sequential NH_3 binding energies of $[Cu(I)(NH_3)_x]^+$ (x = 1–4) in gas phase. This is a system which has been experimentally investigated by collision-induced dissociation [40]. Our calculated (zero-point corrected) sequential binding energies of $[Cu(I)(NH_3)_x]^+$ (x = 1–4) are 2.41, 2.58, 0.51 and 0.41 eV, respectively. This is in good agreement with the experimental values of 2.49, 2.60, 0.52 and 0.42 eV [40], indicating that the Cu–NH_3 bond strength is accurately described by PBE+cx.

For NH_3 adsorption in Cu-CHA, we have considered the species shown in Fig. 1. Figure 1a shows NH_3 adsorbed at a Brønsted acid site forming NH_4^+ and Fig. 1b–f show the different Cu complexes. The sequential desorption energies are reported in Table 1.

Considering the case with adsorbates in each rhombohedral unit cell ($E_{des}^{1\times1\times1}$), the energy required for decomposition of NH_4^+ is calculated to be 1.46 eV, which is within the range (1.34–1.67 eV) measured for the NH_3 adsorption on Brønsted acid sites in H-ZSM-5 [41]. The desorption energies for $[Cu(I)(NH_3)_2]^+$ are 1.29 and 1.54 eV, respectively. The clear separation between the two energies should result in different peaks in the TPD profile. Cu^{2+} is considered with one to four NH_3 ligands. The highest desorption energy is obtained when going from four to three ligands. The sequential desorption energies for the remaining ligands are all lower. Thus, once the decomposition of the $[Cu(II)(NH_3)_4]^{2+}$ complex starts, all ligands should desorb. The situation is slightly more complex for $[Cu(II)(OH)(NH_3)_3]^+$ which shows a non-monotonous behaviour with the highest energy calculated for decompositions of the second NH_3. Thus, also this species should give rise to multiple peaks in the TPD profile.

To study the influence of complex and adsorbate concentration, calculations were performed also in a (2 × 2 × 2) super-cell. In this case, the Si/Al ratio was reduced by a factor of 8 and adsorption was considered only in one of the eight unit cells. The differences in adsorption energies are small, all being within 0.1 eV. In comparison with the high coverage results, cases with Cu-species not directly bonded to the framework, have slightly lower NH_3 adsorption energies, whereas NH_3 bonded to framework-coordinated Cu-ions have slightly higher adsorption energies.

Turning to the TPD profiles, we have simulated desorption curves for some representative cases using the $E_{des}^{1\times1\times1}$ energies. Figure 2a shows the desorption profiles for the linear complex. The peak at ca. 350 °C originates from decomposition of $[Cu(I)(NH_3)_2]^+$, whereas the higher desorption energy for the remaining NH_3 ligand yields a peak at about 460 °C. Figure 2b shows the desorption peaks from NH_4^+ (Brønsted acid site) and $[Cu(II)(NH_3)_4]^{2+}$ at 430 °C and 475 °C, respectively. As the desorption energies of the remaining NH_3 adsorbed on Cu^{2+} are lower than the first, only one peak should appear for this complex.

We compare the simulated TPD profiles with experiments performed for Cu-CHA (Fig. 2c). The experiment was performed with NH_3 adsorbed at 200 °C. The temperature was lowered to 150 °C before starting the TPD measurement. The results show the two features at 290 and

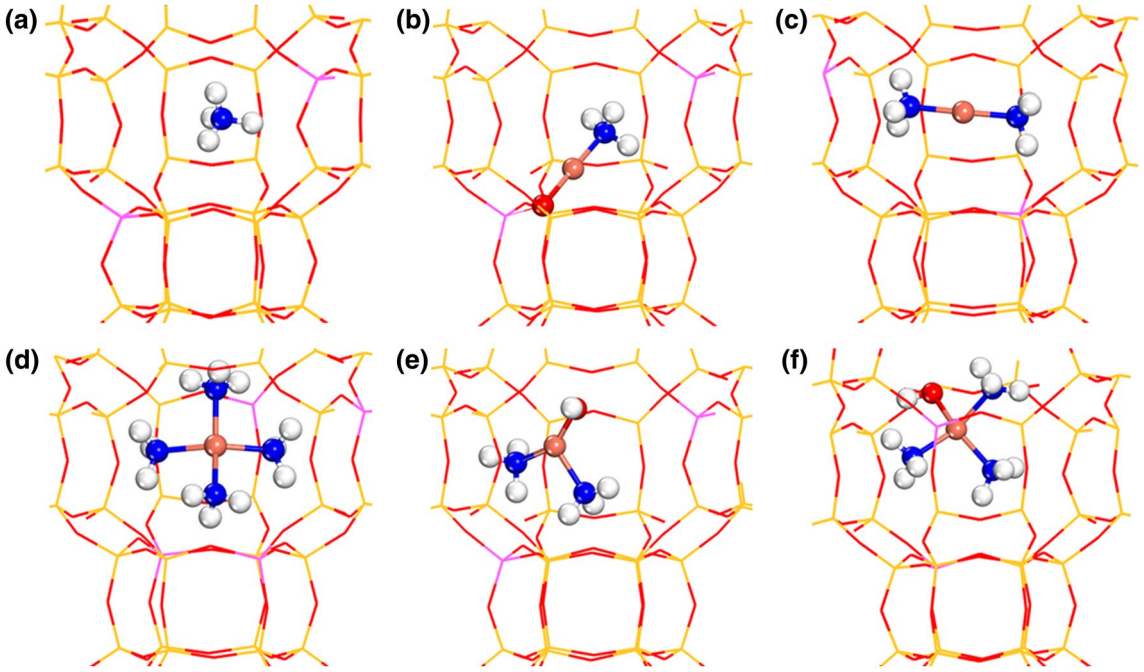

Fig. 1 Selected atomic configurations. **a** NH_4^+, **b** $[Cu(I)NH_3]^+$, **c** linear $[Cu(I)(NH_3)_2]^+$, **d** fourfold $[Cu(II)(NH_3)_4]^{2+}$, **e** $[Cu(II)(OH)(NH_3)_2]^+$ and **f** $[Cu(II)(OH)(NH_3)_3]^+$. Atom color codes: copper (pink), aluminum (purple), nitrogen (blue), silicon (yellow), oxygen (red) and hydrogen (white)

Table 1 The sequential desorption energies from different Cu-complexes in Cu-CHA

Considered desorption processes	$E_{des}^{1\times1\times1}$ (eV)	$E_{des}^{2\times2\times2}$ (eV)
$NH_4^+ \rightarrow H^+ + NH_3(g)$	1.46	1.37
$[Cu(I)(NH_3)_2]^+ \rightarrow [Cu(I)NH_3]^+ + NH_3(g)$	1.29	1.23
$[Cu(I)NH_3]^+ \rightarrow Cu^+ + NH_3(g)$	1.54	1.55
$[Cu(II)(NH_3)_4]^{2+} \rightarrow [Cu(II)(NH_3)_3]^{2+} + NH_3(g)$	1.59	1.51
$[Cu(II)(NH_3)_3]^{2+} \rightarrow [Cu(II)(NH_3)_2]^{2+} + NH_3(g)$	1.07	1.01
$[Cu(II)(NH_3)_2]^{2+} \rightarrow [Cu(II)(NH_3)]^{2+} + NH_3(g)$	0.98	0.88
$[Cu(II)(NH_3)]^{2+} \rightarrow Cu^{2+} + NH_3(g)$	1.36	1.42
$[Cu(II)(OH)(NH_3)_3]^+ \rightarrow [Cu(II)(OH)(NH_3)_2]^+ + NH_3(g)$	0.82	0.74
$[Cu(II)(OH)(NH_3)_2]^+ \rightarrow [Cu(II)(OH)NH_3]^+ + NH_3(g)$	1.20	1.14
$[Cu(II)(OH)NH_3]^+ \rightarrow [Cu(II)(OH)]^+ + NH_3(g)$	0.96	1.00

$E_{des}^{1\times1\times1}$ and $E_{des}^{2\times2\times2}$ corresponds to energies calculated in $1 \times 1 \times 1$ and $2 \times 2 \times 2$ computational cells, respectively. All energies are zero point corrected. Selected configurations are shown in Fig. 1

430 °C, respectively. Based on the calculations, we attribute the lower temperature feature to the decomposition of $[Cu(I)(NH_3)_2]^+$. The feature at higher temperature could be assigned to $[Cu(I)NH_3]^+$, Brønsted acid sites (NH_4^+), and decomposition of $[Cu(II)(NH_3)_4]^{2+}$.

Previously it has been shown that the stability of the $[Cu(I)(NH_3)_2]^+$ pairs depends on the local Al-distribution [24]. Similar effects could be anticipated for complexes considered here, which will lead to a broadening of the TPD features. In addition to the Al-distribution, the concentration of species in the zeolite can give rise to a broadening. The difference between the adsorption energies calculated in the $(1 \times 1 \times 1)$ and the $(2 \times 2 \times 2)$ cells gives an estimate of such effects.

In the literature, three peaks are generally present in the desorption profile of ammonia from Cu-CHA [8–11]. A low-temperature peak below 200 °C, an intermediate-temperature peak at 250–350 °C and a high-temperature peak at 400–500 °C. The intermediate and high-temperature peaks are present in Fig. 2c. It has been suggested that the low-temperature peak should be assigned to NH_3 desorption from Lewis acid sites, the intermediate-temperature

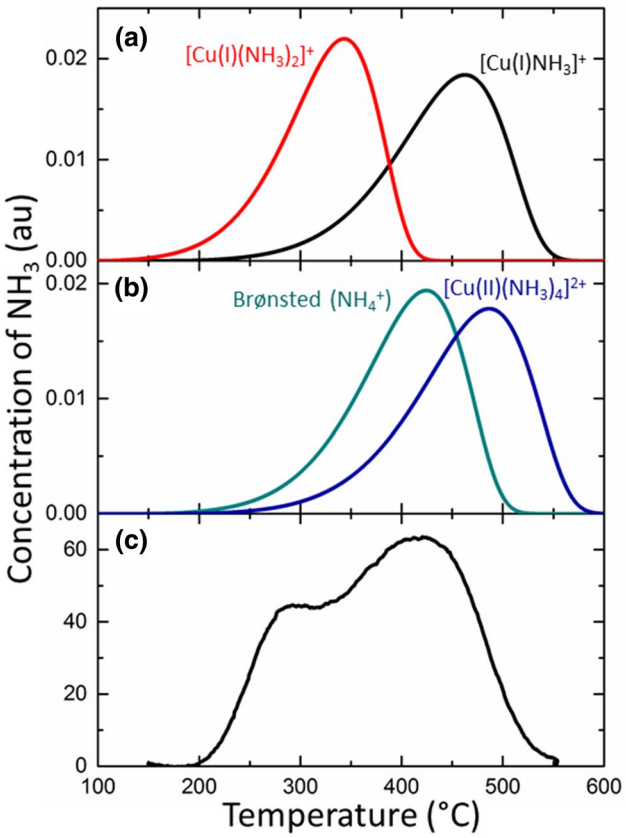

Fig. 2 **a**, **b** Simulated desorption curves of NH_3 in Cu-CHA. The parent complexes are indicated. Only one adsorption event from each complex is considered. **c** Experimental NH_3-TPD profile after NH_3 adsorption in Cu-CHA at 200 °C. The experimental Cu-CHA is prepared with the Si/Al ratio of 15 and the Cu content is 2.6 wt%, which corresponds to a Cu/Al ratio of 0.47. The simulations and experiments are performed with a heating rate of 3 °C/min and a flow rate of 190 Nml/min

peak to Cu-sites and the high-temperature peak to Brønsted acid sites.

Previous thermodynamic analyses [20, 23] together with the present calculations suggest that the three experimentally observed peaks could be attributed to several overlapping features. The low-temperature peak could originate from Lewis acid sites (not analyzed here) and decomposition of $[Cu(II)(OH)(NH_3)_3]^+$. Species that contribute to the intermediate-temperature peak could be the decomposition of the $[Cu(I)(NH_3)_2]^+$ complex and a residual from $[Cu(II)(OH)(NH_3)_3]^+$. The largest overlap is predicted for the high-temperature peak with contributions from Brønsted acid sites (NH_4^+), $[Cu(I)NH_3]^+$ and $[Cu(II)(NH_3)_4]^{2+}$. The contribution of Cu-species to the high-temperature peak, is consistent with the fact that the weight of this peak increases with Cu loading [8].

In addition to assisting the interpretation of the NH_3-TPD, the calculated adsorption energies for Cu^+ and Cu^{2+} species could elucidate the known drop in NH_3-SCR activity with increasing temperature at 300–350 °C. The low-temperature activity is governed by the linear complexes which are known to activate oxygen while forming transient pairs [21–24]. Our calculations show that $[Cu(I)(NH_3)_2]^+$ decomposes at temperatures when the loss of activity is observed. The residual $[Cu(I)NH_3]^+$ species is coordinated to a framework oxygen which hinders activation of O_2. Meanwhile, the $[Cu(II)(NH_3)_4]^{2+}$ complex is still intact and not available for taking part in the catalytic cycle. As the temperature is raised above 350 °C, bare framework coordinated Cu-species are present reactive to oxygen [42]. Thus, NH_3 inhibits the SCR reaction in the intermediate temperature regime.

4 Conclusions

We have used DFT calculations in combination with kinetic simulations to elucidate NH_3-TPD from Cu-CHA. Experimentally, three peaks are generally observed in the desorption profile. A low-temperature peak below 200 °C, an intermediate-temperature peak at 250–350 °C and a high-temperature peak at 400–500 °C. Based on our calculations, the low-temperature peak is assigned to NH_3 desorption from Lewis acid sites together with NH_3 desorption from a $[Cu(II)(OH)(NH_3)_3]^+$ complex. The intermediate-temperature peak is attributed to decomposition of the linear $[Cu(I)(NH_3)_2]^+$ complex and a residual from $[Cu(II)(OH)(NH_3)_3]^+$. The high temperature peak is predicted to have contributions from NH_4^+, $[Cu(I)NH_3]^+$ and $[Cu(II)(NH_3)_4]^{2+}$. A suggestion for the observed NH_3 inhibition of the SCR reaction during intermediate temperatures was discussed based on the calculated NH_3 adsorption energies.

Acknowledgements The Competence Centre for Catalysis is hosted by Chalmers University of Technology and financially supported by the Swedish Energy Agency and the member companies AB Volvo, ECAPS AB, Johnson Matthey AB, Preem AB, Scania CV AB, Umicore Denmark Aps. KG and Volvo Car Corporation AB. Additional financial support from the Swedish Research Council (Grant No. 2016-05234) and the Chalmers Area of Advance Transport is acknowledged. The calculations have been performed at C3SE (Göteborg) and PDC (Stockholm) through a SNIC grant.

References

1. Centi G, Perathoner S, Trifiro F, Aboukais A, Aissi C, Guelton M (1992) Physicochemical characterization of V-silicalite. J Phys Chem 96:2617–2629
2. Lónyi F, Valyon J (2001) On the interpretation of the NH_3-TPD patterns of H-ZSM-5 and H-mordenite. Microporous Mesoporous Mater 47:293–301
3. Srivastava RK, Neuffer W, Grano D, Khan S, Staudt JE, Jozewicz W (2005) Controlling NO_x emission from industrial sources. Environ Prog 24:181–197
4. Beale AM, Gao F, Lezcano-Gonzalez I, Peden CH, Szanyi J (2015) Recent advances in automotive catalysis for NO_x emission control by small-pore microporous materials. Chem Soc Rev 44:7371–7405
5. Kwak JH, Tonkyn RG, Kim DH, Szanyi J, Peden CH (2010) Excellent activity and selectivity of Cu-SSZ-13 in the selective catalytic reduction of NO_x with NH_3. J Catal 275:187–190
6. Schmieg SJ, Oh SH, Kim CH, Brown DB, Lee JH, Peden CH, Kim DH (2012) Thermal durability of Cu-CHA NH_3-SCR catalysts for diesel NO_x reduction. Catal Today 184:252–261
7. Gao F, Walter ED, Karp EM, Luo J, Tonkyn RG, Kwak JH, Szanyi J, Peden CH (2013) Structure-activity relationships in NH_3-SCR over Cu-SSZ-13 as probed by reaction kinetics and EPR studies. J Catal 300:20–29
8. Leistner K, Xie K, Kumar A, Kamasamudram K, Olsson L (2017) Ammonia desorption peaks can be assigned to different copper sites in Cu/SSZ-13. Catal Lett 147:1882–1890
9. Fan C, Chen Z, Pang L, Ming S, Zhang X, Albert K, Liu P, Chen H, Li T (2018) The influence of Si/Al ratio on the catalytic property and hydrothermal stability of Cu-SSZ-13 catalysts for NH_3-SCR. Appl Catal A 550:256–265
10. Luo J, Gao F, Kamasamudram K, Currier N, Peden C, Yezerets A (2017) New insights into Cu/SSZ-13 SCR catalyst acidity. Part I: nature of acidic sites probed by NH_3 titration. J Catal 348:291–299
11. Gao F, Washton N, Wang Y, Kollár M, Szanyi J, Peden C (2015) Effects of Si/Al ratio on Cu/SSZ-13 NH_3-SCR catalysts: implications for the active Cu species and the roles of Brønsted acidity. J Catal 331:25–38
12. Gao F, Wang Y, Washton N, Kollár M, Szanyi J, Peden C (2015) In situ-DRIFTS study of selective catalytic reduction of NO_x by NH_3 over Cu-exchanged SAPO-34. ACS Catal 5:6780–6791
13. Ma L, Su W, Li Z, Li J, Fu L, Hao J (2015) Mechanism of propene poisoning on Cu-SSZ-13 catalysts for SCR of NOx with NH_3. Catal Today 245:16–21
14. Zhang T, Qiu F, Chang H, Li X, Li J (2016) Identification of active sites and reaction mechanism on low-temperature SCR activity over Cu-SSZ-13 catalysts prepared by different methods. Catal Sci Technol 6:6294–6304
15. Giordanino F, Borfecchia E, Lomachenko K, Lazzarini A, Agostini G, Gallo E, Soldatov A, Beato P, Bordiga S, Lamberti C (2014) Interaction of NH_3 with Cu-SSZ-13 catalyst: a complementary FTIR, XANES, and XES study. J Phys Chem Lett 5:1552–1559
16. Zhu H, Kwak J, Peden C, Szanyi J (2013) In situ DRIFTS-MS studies on the oxidation of adsorbed NH_3 by NO_x over a Cu-SSZ-13 zeolite. Catal Today 245:16–23
17. Lezcano-Gonzalez I, Deka U, Arstad B, Van Yperen-De Deyne A, Hemelsoet K, Waroquier M, Van Speybroeck V, Weckhuysen B, Beale A (2014) Determining the storage, availability and reactivity of NH_3 within Cu-chabazite-based ammonia selective catalytic reduction systems. Phys Chem Chem Phys 16:1639–1650
18. Marberger A, Petrov A, Steiger P, Elsener M, Kröcher O, Nachtegaal M, Ferri D (2018) Time-resolved copper speciation during selective catalytic reduction of NO on Cu-SSZ-13. Nat Catal 1:221–227
19. Lomachenko K, Borfecchia E, Negri C, Berlier G, Lamberti C, Beato P, Falsig H, Bordiga S (2016) The Cu-CHA deNO $_x$ catalyst in action: temperature-dependent NH_3-assisted selective catalytic reduction monitored by operando XAS and XES. J Am Chem Soc 138:12025–12028
20. Paolucci C, Parekh AA, Khurana I, Di Iorio JR, Li H, Albarracin Caballero JD, Shih AJ, Anggara T, Delgass WN, Miller JT, Ribeiro FH, Gounder R, Schneider WF (2016) Catalysis in a cage: condition-dependent speciation and dynamics of exchanged Cu cations in SSZ-13 zeolites. J Am Chem Soc 138:6028–6048
21. Gao F, Mei D, Wang Y, Szanyi J, Peden C (2017) Selective catalytic reduction over Cu/SSZ-13: linking homo-and heterogeneous catalysis. J Am Chem Soc 139:4935–4942
22. Paolucci C, Khurana I, Parekh AA, Li S, Shih AJ, Li H, Di Iorio JR, Albarracin-Caballero JD, Yezerets A, Miller JT, Delgass WN, Ribeiro FH, Schneider WF, Gounder R (2017) Dynamic multinuclear sites formed by mobilized copper ions in NO_x selective catalytic reduction. Science 357:898–903
23. Chen L, Falsig H, Janssens T, Grönbeck H (2018) Activation of oxygen on $(NH_3\text{-}Cu\text{-}NH_3)^+$ in NH_3-SCR over Cu-CHA. J Catal 358:179–186
24. Chen L, Falsig H, Jansson J, Janssens T, Skoglundh M, Grönbeck H (2018) Effect of Al-distribution on oxygen activation over Cu-CHA. Catal Sci Technol 8:2131–2136
25. Chen L, Jansson J, Skoglundh M, Grönbeck H (2016) Mechanism for solid-state ion exchange of Cu^+ into zeolites. J Phys Chem C 120:29182–29189
26. Kresse G, Hafner J (1993) Ab initio molecular dynamics for open-shell transition metals. Phys Rev B 48:13115–13118
27. Kresse G, Hafner J (1994) Ab initio molecular-dynamics simulation of the liquid-metal-amorphous-semiconductor transition in germanium. Phys Rev B 49:14251–14269
28. Kresse G, Furthmüller J (1996) Efficient iterative schemes for ab initio total-energy calculations using a plane-wave basis set. Phys Rev B 64:11169–11186
29. Kresse G, Furthmüller J (1996) Efficiency of ab-initio total energy calculations for metals and semiconductors using a plane-wave basis set. J Comput Mater Sci 6:15–50
30. Blöchl PE (1994) Projector augmented-wave method. Phys Rev B 50:17953–17979
31. Kresse G, Joubert D (1999) From ultrasoft pseudopotentials to the projector augmented-wave method. Phys Rev B 59:1758–1775
32. Berland K, Hyldgaard P (2014) Exchange functional that tests the robustness of the plasmon description of the van der Waals density functional. Phys Rev B 89:035412
33. Lee K, Murray ED, Kong L, Lundqvist BI, Langreth DC (2010) Higher-accuracy Van Der Waals density functional. Phys Rev B 82:8207–8215
34. Clemens AK, Shishkin A, Carlsson P-A, Skoglundh M, Martínez-Casado FJ, Matěj Z, Balmes O (2015) Reaction-driven ion exchange of copper into zeolite SSZ-13. ACS Catal 5:6209–6218
35. Shishkin A, Kannisto H, Carlsson PA, Härelind H, Skoglundh M (2014) Synthesis and functionalization of SSZ-13 as an NH_3 -SCR catalyst. Catal Sci Technol 4:3917–3926
36. Eilertsen EA, Nilsen MH, Wendelbo R, Olsbye U, Lillerud KP (2008) Synthesis of high silica CHA zeolites with controlled Si/Al ratio. Stud Surf Sci Catal 174:265–268

37. Niwa M, Katada N, Sawa M, Murakami Y (1995) Temperature-programmed desorption of ammonia with readsorption based on the derived theoretical equation. J Phys Chem 99:8812–8816
38. Katada N, Igi H, Kim J, Niwa M (1997) Determination of the acidic properties of zeolite by theoretical analysis of temperature-programmed desorption of ammonia based on adsorption equilibrium. J Phys Chem B 101:5969–5977
39. Janssens T, Falsig H, Lundegaard L, Vennestrøm P, Rasmussen S, Moses P, Giordanino F, Borfecchia E, Lomachenko K, Lamberti C, Bordiga S (2015) A consistent reaction scheme for the selective catalytic reduction of nitrogen oxides with ammonia. ACS Catal 5:2832–2845
40. Walter D, Armentrout PB (1998) Sequential bond dissociation energies of $M^{+}(NH_3)_x$ (x = 1–4) for M = TiCu. J Am Chem Soc 120:3176–3187
41. Rodríguez-González L, Hermes F, Bertmer M, Rodríguez-Castellón E, Jiménez-López A, Simon U (2007) The acid properties of H-ZSM-5 as studied by NH^3-TPD and ^{27}Al-MAS-NMR spectroscopy. Appl Catal A 328:174–182
42. Falsig H, Vennestrøm P, Moses P, Janssens T (2016) Activation of oxygen and NO in NH_3-SCR over Cu-CHA catalysts evaluated by density functional theory. Catal Today 59:861–865